Confirmation of Multiple Pattern Speeds in the Barred, Grand Design Spiral Galaxy NGC 4321

Nick Wade & Jason Speights
Frostburg State University

Abstract

Previous measurements of the pattern speed in NGC 4321 show evidence for a pattern speed that decreases with increasing radius. These measurements used a version of the Tremaine-Weinberg method that assumes a constant value of the pattern speed across the disk, so we checked those results using a general form of the method that excludes the assumption of a constant pattern speed. We find 3 approximately constant values of the pattern speed for the nuclear, bar, and spiral arms, consistent with previous measurements, but our values for the nuclear and bar regions are larger. The larger values are explainable as due to the bias from averaging when applying the version of the method that assumes a constant value of the pattern speed. Our results are consistent with mode coupling of the bar and the beginning of the spirals at the 4:1 ultraharmonic resonance.

Background

H05a find evidence for different pattern speeds (Ω_p) using the original form of the TW84 method. The original method assumes the disk is flat, Ω_p is constant with increasing radius, and the tracer of the pattern used obeys mass conservation in the continuity equation. Their result,

$$\int_{-\infty}^{+\infty} I(x,y)\, V_y(x,y)\, dx = \Omega_p \int_{-\infty}^{+\infty} I(x,y)\, x\, dx, \qquad (1)$$

relates Ω_p to the observable intensity, I, and the line-of-sight velocity, V_{los}, corrected for the systemic velocity, V_{sys}, and disk inclination angle, ϕ_i,

$$V_y = \frac{V_{los} - V_{sys}}{\sin(\phi_i)}. \qquad (2)$$

Our Methods

We used a general form of the TW84 method,

$$\int_{-\infty}^{+\infty} I(x,y)\, V_y(x,y)\, dx = \int_{\pm y}^{+\infty} \Omega_p(r)\, \{ I(\sqrt{r^2-y^2}, y) - I(-\sqrt{r^2-y^2}, y) \}\, r\, dr, \qquad (3)$$

that allows for Ω_p to vary with radius (E94, M06). Stable solutions of this integral equation are found using first order Tikhonov regularization (A05).

Before applying our methods, we adopted or measured many parameters of NGC 4321. The kinematic center and ϕ_i are adopted from the NED and H05b, respectively. The disk position angle, ϕ_p, and V_{sys}, are found by fitting models to the velocity field. To find ϕ_p, we fit a model of the form,

$$V_{los}(r,\theta) = V_{sys} + V_\theta(r)\cos(\theta)\sin(\phi_i) \qquad (4)$$

where that V_θ is the circular speed and,

$$\cos(\theta) = \frac{\triangle\alpha \sin(\phi_p) + \triangle\delta \cos(\phi_p)}{r}. \qquad (5)$$

The value of ϕ_p that produces a global minimum in the sum of the squared residuals (SSR) is adopted for finding Ω_p, and the associated value of V_{sys} is used in equation (2).

Data

The data are H-alpha I and V_{los} maps from H05b. They observed NGC 4321 using a Fabry-Perot integral-field spectrometer on the 1.6 meter telescope of the Observatoire du Mont-Mégantic.

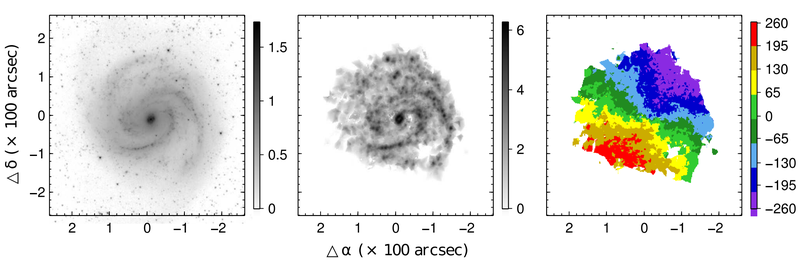

Fig. 1 From left to right is a 3.6 micrometer image from K03, h-alpha intensity, and corrected h-alpha velocity. The units shown for the 3.6 micrometer and h-alpha intensity images are log(counts). The corrected velocity is shown in bins of 65 km s^{-1}.

Results

Position Angle

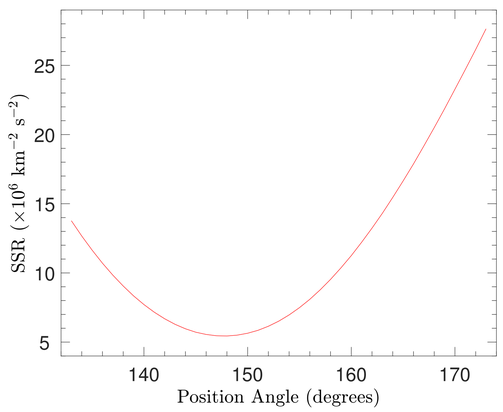

Fig. 2 Sum of squared residuals for a range of ϕ_p. Note the global minimum at ϕ_p = 147.7°.

Rotation Curve

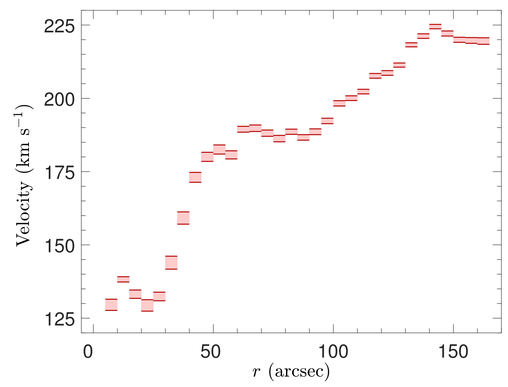

Fig. 3 Rotation curve using 5 arcsecond rings. The red line segments show the upper and lower bounds of the 95% confidence intervals for V_θ.

Pattern Speed

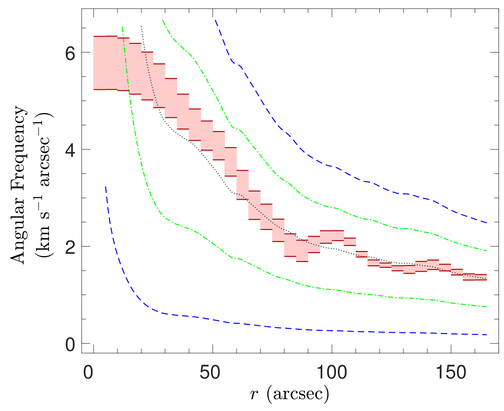

Fig. 4 Pattern speed results using 5 arcsecond rings. The red line segments show the upper and lower bounds of the 95% confidence intervals for Ω_p. The dotted black line, dash-dot green lines, and dashed blue lines show possible locations for corotation, m=4 Lindblad resonance, and m=2 Lindblad resonance, respectively.

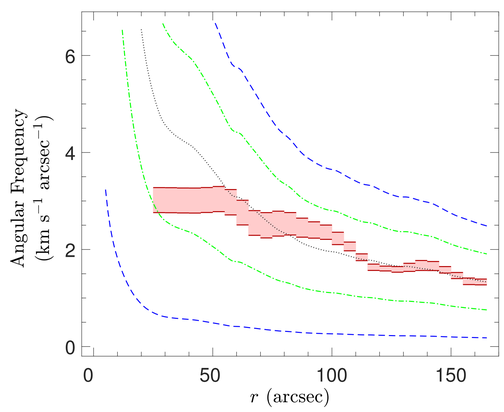

Fig. 5 Pattern speed results for a solution that excludes the innermost 25 arcseconds of the disk. The figure is formatted in the same way as figure 4.

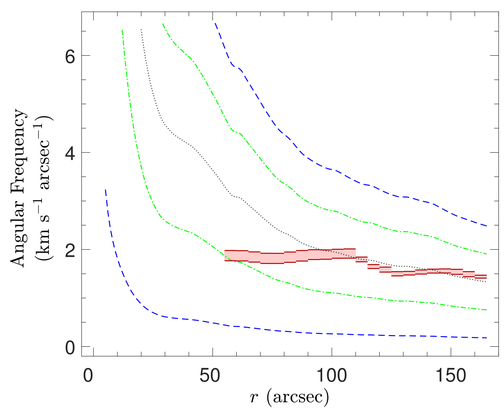

Fig. 6 Pattern speed results for a solution that excludes the innermost 55 arcseconds of the disk. The figure is formatted in the same way as figure 4.

Three pattern speed solutions are found for the purpose of distinguishing the nuclear, bar, and spiral regions of the galaxy. A solution for the whole disk is used for the nuclear region. Solutions that exclude integration paths crossing over the innermost 25 arcseconds, and innermost 55 arcseconds, are used for the bar and spiral regions, respectively. Excluding these regions reduces the bias from regularization.

<u>These results appear to be consistent with mode coupling at the ultraharmonic resonance (T87, MT97).</u> The bias from regularization, however, excludes a definitive conclusion based on these results alone.

Discussion

Elliptical Flow Model

We used an elliptical flow model of the form,

$$V_y(r,\theta) = V_{\theta 0}(r)\cos(\theta) - V_{\theta 2}(r)\cos(\theta)\cos(2[\theta-\phi_o]) - V_{r2}(r)\sin(\theta)\sin(2[\theta-\phi_o]), \qquad (6)$$

(SS07) to test the results for the bar region. The value of the phase angle for the position of the bar, ϕ_o, is adopted from SM18. From this model we can estimate,

$$\Omega_p' = \frac{V_{\theta 0} - V_{\theta 2}}{r}. \qquad (7)$$

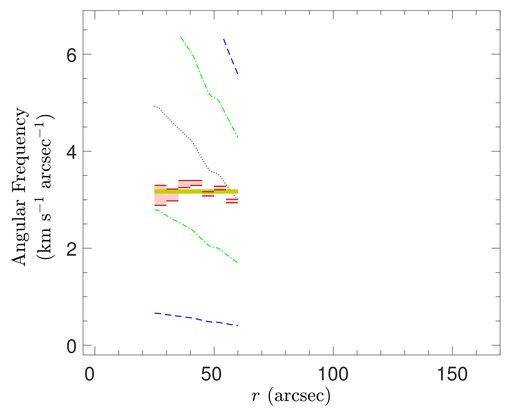

Fig. 7 Pattern speed results for the elliptical flow model. The figure is formatted similar to figure 4, with the addition of a gold shaded line showing the 95% confidence intervals for the mean of Ω_p'

Comparison with previous TW results

The lower values found by H05a are explainable due to the averaging that occurs when the original method is applied to a radially varying pattern speed. The larger value for the elliptical flow model is possibly due to the bias caused by regularization. Despite these differences, the similarities are compelling.

Comparison of Results

Region	H05a	This Work	
		TW	Elliptical Flow Model
Nuclear	4.30 ± 1.00	5.70 ± 0.14	
Bar	2.30 ± 0.18	3.02 ± 0.01	3.17 ± 0.04
Spiral	1.60 ± 0.06	1.87 ± 0.02	

In units of km s^{-1} arcsec–1.

Acknowledgements

The results in the poster are from a Senior Seminar and Capstone course at Frostburg State University (FSU). Funding was provided by FSU in the form of a Provost's Experiential Learning Enhancement Fund Grant, and an Undergraduate Student Travel Grant. This research has made use of the Fabry Perot database, operated at CeSAM/LAM, Marseille, France. This research has made use of the NASA/IPAC Extragalactic Database (NED) which is operated by the Jet Propulsion Laboratory, California Institute of Technology, under contract with the National Aeronautics and Space Administration.

References

Aster, R. C., Borchers, B., & Thurber, C. H. 2005, Parameter Estimation and Inverse Problems (San Diego, CA: Elsevier Academic) (A05)
Engstroem, S. 1994, A&A, 285, 801 (E94)
Hernandez, O., Carignan, C., Amram, P., Chemin, L., & Daigle, O. 2005, MNRAS, 360, 1201 (H05a)
Hernandez, O., Wozniak, H., Carignan, C., et al. 2005, AJ, 632, 253 (H05b)
Kennicutt, R. C., Jr, Armus, L., Bendo, G., et al. 2003, PASP, 115, 928 (K03)
Masset, F., & Tagger, M. 1997, A&A, 322, 442 (MT97)
Merrifield, M. R., Rand, R. J., & Meidt, S. E. 2006, MNRAS, 366, L17 (M06)
Speights, J., & Mooney, C. 2018, in American Astronomical Society Meeting Abstracts, Vol 231, 248.06 (SM18)
Spekkens, K., & Sellwood, J. A. 2007, ApJ, 664, 204 (SS07)
Tagger, M., Synget, J. F., Athanassoula, E., & Pellat, R. 1987, ApJ, 318, L43 (T87)
Tremaine, S., & Weinberg, M. D. 1984, ApJ, 282, L5 (TW84)